

# Computer assisted early detection of liver metastases from fMRI maps

M. Freiman<sup>a</sup>, Y. Edrei<sup>b,c</sup>, E. Gross<sup>d</sup>, L. Joskowicz<sup>a</sup>, R. Abramovitch<sup>b,c</sup>

<sup>a</sup>*School of Engineering and Computer Science, The Hebrew University of Jerusalem, Israel.*

<sup>b</sup>*The Goldyne Savad Inst. for Gene Therapy, Hadassah Hebrew University Medical Center, Jerusalem, Israel.*

<sup>c</sup>*MRI/MRS lab HBRC, Hadassah Hebrew University Medical Center, Jerusalem, Israel.*

<sup>d</sup>*Pediatric Surgery, Hadassah Hebrew University Medical Center, Jerusalem, Israel.*

**Abstract.** We present a new method for computer-aided early detection of liver metastases tumors. The method characterized colorectal hepatic metastases and follows their early hemodynamical changes using an fMRI-based statistical model. The changes in hepatic hemodynamics are evaluated from T<sub>2</sub>W fMRI images acquired during breathing of air, air-CO<sub>2</sub>, and carbogen. A classification model is build to help radiologists differentiate tumor from healthy tissue. The model is built from 132 well-validated fMRI samples of tumors and healthy tissue. For each sample, a histogram-based features-vector is constructed. The model is then generated from the data with an SVM classifier. To test the model, 32 non-validated fMRI samples were used. 22 samples proved to be healthy tissue and 11 samples proved to be tumors. 9 samples were judged as tumors by the naked eye, but proved to be healthy tissue later. Our classification model yields accuracy of 78.12% with 66.67% precision on the test set.

*Keywords: Computer aided early detection, fMRI analysis, liver tumors, tumor statistical model*

---

## 1. Introduction

The liver is the most common site of visceral metastasis for colorectal carcinoma patients, with hepatic metastases a frequent clinical complication. Despite the availability of numerous treatments, hepatic metastases are difficult to eradicate because of their late discovery. It is well known that, whereas normal liver is supplied predominantly by the portal vein, in patients with overt colorectal liver metastases, a higher proportion of liver blood flow comes from the hepatic artery [1]. Thus, earlier detection of hepatic metastases may be feasible by monitoring hemodynamical changes.

The association between hepatic metastases and altered liver blood flow has been demonstrated by dynamic scintigraphy [1], by Doppler sonography [2,3], by dynamic contrast enhanced CT [4] and more recently, by dynamic contrast enhanced MRI [5]. Measurements using MRI can potentially overcome limitations posed by other imaging techniques, such as poor spatial resolution in radionuclide studies, lack of reproducibility in Doppler US and radiation exposure using CT. Today, in order to acquire perfusion images in both CT and MRI there is a need to use intravenous administration of contrast agent. Good separation of arterial from portal phase requires high temporal resolution which enforces reduction of the spatial resolution.

Recently, we demonstrated the feasibility of fMRI utilizing hypercapnia and hyperoxia for monitoring changes in liver perfusion and haemodynamics without the need of contrast agent administration [6]. Using this method we characterized colorectal hepatic metastases and we followed their early hemodynamical changes [7]. However, it is hard to isolate regions in the image with significant hemodynamic changes in data sets acquired at early phase of tumor development.

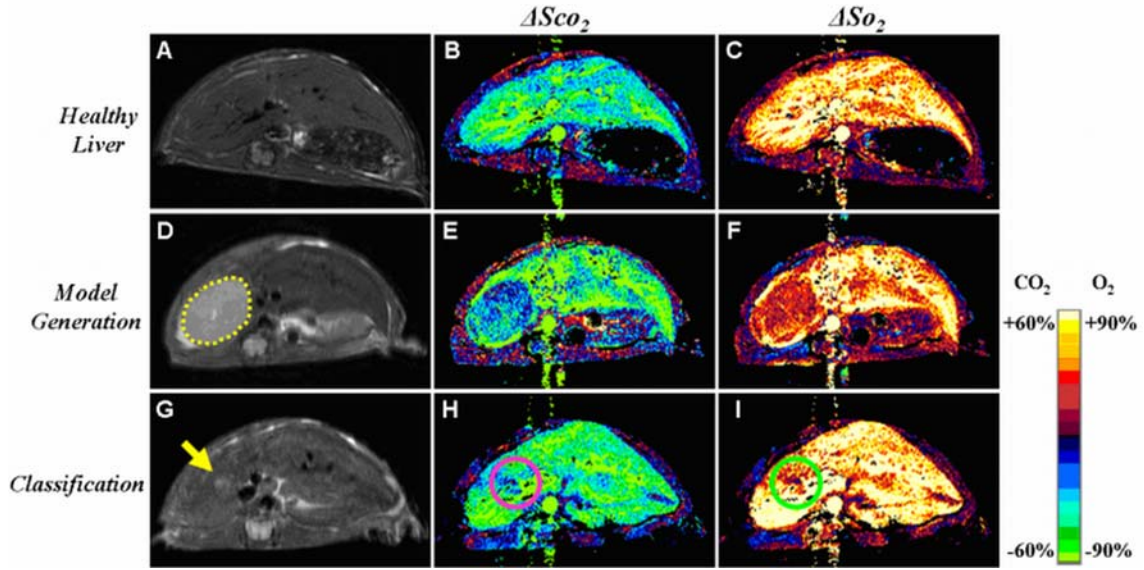


Fig. 1. Representative T<sub>2</sub>W anatomical images (Left),  $\Delta S_{CO_2}$  maps (Centre) and  $\Delta S_{O_2}$  maps (Right) of mice livers ( $\Delta S$  values as indicated in color-bar). Healthy liver (A-C); Confirmed tumor (D, yellow circle) from late phase growth (21 days following cell injection) that was taken for model generation (D-F); Suspected area (G, yellow arrow) from early phase growth (14 days following cell injection) that was taken for classification. Note typical changes in the corresponding  $\Delta S$  maps (circled area in H, I).

## 2. Methods

This paper presents a new method for the identification and classification of regions with significant hemodynamic changes in fMRI images at the early tumor development stage. The method automatically classifies early fMRI studies based on a learned model of tumors constructed from validated training datasets. We propose a two-phase method consisting of a model generation from training datasets of anatomical and fMRI images with tumors and a classification of new fMRI images based on the generated model.

The model generation (training) phase proceeds as follows. The input training set consists of a series of datasets of live subjects (mice) with and without tumors. Each dataset consists of four images: an anatomical MRI image (*MRI*) and three fMRI maps. The fMRI maps were computed by taking the mean of eight acquisitions in normal conditions ( $\bar{S}_{air}$ ) and during the inhalation of CO<sub>2</sub> ( $\bar{S}_{CO_2}$ ) and oxygen ( $\bar{S}_{O_2}$ ). In the first step, two signal intensity maps are computed from the three fMRI maps to measure the percentage of change of the fMRI signal intensity induced by hypercapnia ( $\Delta S_{CO_2}$ ) and hyperoxia ( $\Delta S_{O_2}$ ) as follows:

$$\Delta S_{CO_2} = \frac{\bar{S}_{CO_2} - \bar{S}_{air}}{\bar{S}_{air}} \times 100, \quad \Delta S_{O_2} = \frac{\bar{S}_{O_2} - \bar{S}_{CO_2}}{\bar{S}_{CO_2}} \times 100$$

where the images are represented as pixel matrices and the computation is for each pixel. An example of the resulting  $\Delta S_{CO_2}$  and  $\Delta S_{O_2}$  image maps is shown in Fig 1.

Next, for each  $\Delta S_{CO_2}$  and  $\Delta S_{O_2}$  image map, one or more Regions of Interest (ROIs) suspected of containing tumors are manually identified. For each ROI, a one-dimensional histogram of the intensity values is computed. The size of the square region containing the tumor varies from region to region and is chosen to match the tumor size and shape. Both histograms are generated with a fixed number of bins and are normalized according to the number of pixels in the region. Then, for each region and its associated pair of one-dimensional histograms, we compute an  $n$ -dimensional

features-vector by concatenating the histogram vectors into a single vector. We use the histograms instead of the pixel vectors themselves as feature vectors to obtain a normalized measure independent of tumor size and shape.

The training step then proceeds as follows: for each region, the radiologist manually identifies the ROI in the anatomical MRI image and classifies it as either healthy (no tumor, Fig 1A) or pathological (tumor, Fig. 1D). The software computes the corresponding features-vector from the  $\Delta S_{O_2}$  and  $\Delta S_{CO_2}$  image maps (Fig 1 B,C for healthy tissue, and Fig 1 E,F for pathological tissue). A Support Vector Machine (SVM) classification engine [8] produces from this training set a tumor model consisting of an n-dimensional discriminative hyper-plane between regions with and without tumors.

The early detection step proceeds as follows. Three fMRI images of the new specimen are acquired before the tumor has grown. From the three images, the  $\Delta S_{CO_2}$  and  $\Delta S_{O_2}$  image maps (Fig 1 H,I) , their Regions of Interest (ROIs), and their corresponding features vectors are computed as in the previous phase. The features vector is then classified according to the tumor classification model produced in the training step. The radiologist can evaluate both the yes/no answer for each ROI and the distance of the suspected region from the discriminative hyper-plane. In our experiments the result of the classification is also validated at a later time (several days or weeks later), once the potential tumor has had time to develop. An anatomical MRI image or histology of the ROI is taken and its result compared with that of the classification.

### 3. Experiment and results

We performed an animal study on CB6F1 mice that underwent splenic injection with CT-26 colon cancer cells ( $10^4$  cells/mouse in 0.3 ml) to generate metastases. The spleen is removed 5 min later. In this model, 1-5 hepatic nodules were detected 13-15 days after cell inoculation by using T<sub>2</sub>W fast SE. Tumor progression was monitored twice a week by MRI. Animals were sacrificed, and livers were taken for histology.

For the images, we used a 4.7T Bruker Biospec spectrometer with a bird cage coil. Hepatic volumetric assessment is acquired by serial coronal and axial T<sub>1</sub>-weighted SE images (TR/TE=250/18ms). Tumor assessment was done using T<sub>2</sub>-weighted fast SE images (TR/TE=2000/40ms). Changes in hepatic hemodynamics were evaluated from T<sub>2</sub>\*-weighted GE (TR/TE=147/10ms) images acquired during breathing of air, air-CO<sub>2</sub> (5% CO<sub>2</sub>), and carbogen (95% oxygen; 5% CO<sub>2</sub>), 8 repeats for each gas.

For model generation, we build a database that contains 128 samples of  $\Delta S_{CO_2}$  and  $\Delta S_{O_2}$  maps. The database includes 64 samples of confirmed tumors and 64 samples of healthy livers. For each sample we generated its features-vector, where the features were the intensity histograms of both  $\Delta S_{CO_2}$  and  $\Delta S_{O_2}$  maps, with 8 bins per histogram. We then generated a 16-dimensional classification model using a SVM engine with a polynomial kernel [9]. Then, we classified 32 cases of  $\Delta S$  maps that were acquired at the early tumor growth phase. In all of those cases, no tumors were visible in the anatomical images (T<sub>2</sub>-weighted) at that point in time (between days 10-15 after tumor cells injection). From the 32 cases, 11 were confirmed as tumors at later time points with anatomical images of the same position, and 21 cases showed a healthy liver. From the 21 negative cases, 9 had “tumor-like”  $\Delta S$  maps when observed with the naked eye.

These samples were classified according to the generated model and validated later by MRI or by histology. We checked our test set according to the model using the three types of features described above. We compiled the results using Receiver Operator Characteristics (ROC) graphs [10], as shown in Fig 2. The best results were obtained by

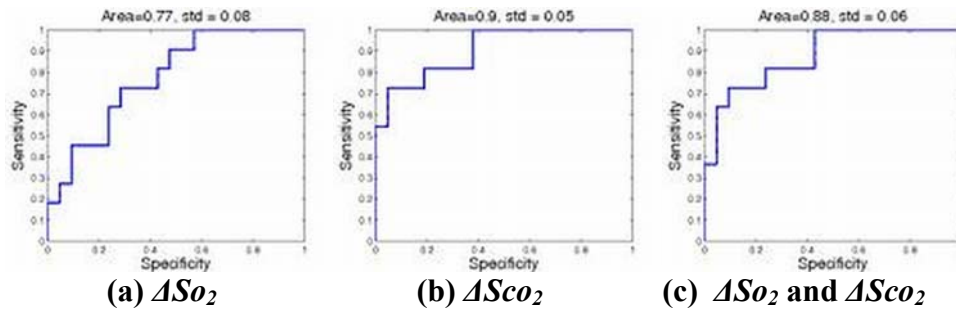


Fig. 2. ROC curves of the classification results using different features.

using  $\Delta SCO_2$  features solely, with accuracy of 78.12%, precision of 66.67%. The best recall of 81.82% was obtained by using both  $\Delta SCO_2$  and  $\Delta SO_2$ .

#### 4. Conclusion

This paper presented a novel method for early detection of liver metastases using computerized analysis of fMRI images. The analysis uses histogram-based features-vector and an SVM classifier to produce a tumor model. The above classification model provide better results than the “naked eye” decisions regarding tumor existence at early time points, where tumors are not detectable in anatomical images. The accuracy of this classification model is high (78%) and the number of false-positive cases is much lower than ours (4 cases with the model vs. 9 cases with human eyes). These results emphasize the necessity for a machine learning tool for enhanced and earlier diagnosis of liver tumors, which hopefully would improve prognosis.

#### References

1. Leveson S, Wiggins P, Giles G, Parkin A, Robinson P. Deranged blood flow patterns in the detection of liver metastases. *British Journal of Surgery*. 1985 February;72:128–130.
2. Leen E, Goldberg J, Robertson J, et al. Early detection of occult colorectal hepatic metastases using duplex colour Doppler sonography. *British Journal of Surgery*. 1993 October;80:1249–1251.
3. Yarmenitis SD, Kalogeropoulou CP, Hatjikondi O, et al. An experimental approach of the Doppler perfusion index of the liver in detecting occult hepatic metastases: histological findings related to the hemodynamic measurements in Wistar rats. *European Radiology*. 2000 February;10(3):417–424.
4. Cuenod CA, Leconte I, Siauve N, et al. Early Changes in Liver Perfusion Caused by Occult Metastases in Rats: Detection with Quantitative CT. *Radiology*. 2001;218(2):556–561.
5. Totman JJ, O’Gorman RL, Kane PA, Karani JB. Comparison of the hepatic perfusion index measured with gadolinium-enhanced volumetric MRI in controls and in patients with colorectal cancer. *British Journal of Radiology*. 2005;78(926):105–109.
6. Barash H, Gross E, Matot I, et al. Functional-MRI during hypercapnia and hyperoxia: a non-invasive monitoring tool for changes in liver perfusion and hemodynamics in a rat model. *Radiology*. 2007; In press.
7. Edrei Y, Gross E, Pikarsky E, Galun E, Abramovitch R. Characterization and Early Detection of Liver Metastasis by fMRI; 2006. Abstract no. 1752. *Proc. 14th Int. Soc. Magnetic Resonance in Medicine (ISMRM)*.
8. Vapnik VN. *The nature of statistical learning theory*. New York, USA: Springer-Verlag, Inc.; 1995.
9. Joachims T. Making large-scale support vector machine learning practical. In: Schölkopf B, Burges C, Smola A, editors. *Advances in kernel methods: support vector learning*. Cambridge, MA, USA: MIT Press; 1999. p. 169–184.
10. T. Fawcett, ROC graphs: Notes and practical considerations for data mining researchers, *Hewlett-Packard Internal Research Report*, 2003.